JB
Journals.ASM.org

Francisella tularensis RipA Protein Topology and Identification of Functional Domains

Brittany L. Mortensen, James R. Fuller, Sharon Taft-Benz, Edward J. Collins, and Thomas H. Kawula

Department of Microbiology and Immunology, School of Medicine, University of North Carolina at Chapel Hill, Chapel Hill, North Carolina, USA

Francisella tularensis is a Gram-negative coccobacillus and is the etiological agent of the disease tularemia. Expression of the cytoplasmic membrane protein RipA is required for *Francisella* replication within macrophages and other cell types; however, the function of this protein remains unknown. RipA is conserved among all sequenced *Francisella* species, and RipA-like proteins are present in a number of individual strains of a wide variety of species scattered throughout the prokaryotic kingdom. Crosslinking studies revealed that RipA forms homoligomers. Using a panel of RipA-green fluorescent protein and RipA-PhoA fusion constructs, we determined that RipA has a unique topology within the cytoplasmic membrane, with the N and C termini in the cytoplasm and periplasm, respectively. RipA has two significant cytoplasmic domains, one composed roughly of amino acids 1 to 50 and the second flanked by the second and third transmembrane domains and comprising amino acids 104 to 152. RipA functional domains were identified by measuring the effects of deletion mutations, amino acid substitution mutations, and spontaneously arising intragenic suppressor mutations on intracellular replication, induction of interleukin-1β (IL-1β) secretion by infected macrophages, and oligomer formation. Results from these experiments demonstrated that each of the cytoplasmic domains and specific amino acids within these domains are required for RipA function.

*F*rancisella tularensis is a Gram-negative coccobacillus that is the etiological agent of the zoonotic disease tularemia. *F. tularensis* infects a wide range of hosts, which includes humans, but predominately infects small mammals such as rabbits, voles, and squirrels (24). *F. tularensis* has been isolated from arthropod vectors such as ticks (29, 34), mosquitoes (28, 43), and deerflies (24), which are also a source of transmission to humans (5, 6). Additional modes of transmission to humans include contact with infected animals (30, 31, 36), ingestion of contaminated food or water (23, 25), and inhalation of aerosolized bacteria (37, 42). There are four main subspecies of *F. tularensis* that differ in their virulence for humans: *F. tularensis* subsp. *novicida*, *mediasiatica*, *holarctica*, and *tularensis*. *F. tularensis* subsp. *novicida* is not generally considered pathogenic for humans; however, there have been a few cases reported (1, 9, 20, 26). *F. tularensis* subsp. *mediasiatica* is associated with human disease in Asia, though less is understood about its pathogenesis (24). *F. tularensis* subsp. *holarctica* and *tularensis* are most commonly associated with disease in humans, with the latter being associated with the lowest infectious dose and most severe disease. For *F. tularensis* subsp. *tularensis*, transmission to humans via the inhalational route can occur at an infectious dose of as few as 10 organisms (35). The ease of aerosolization and low infectious dose resulted in the designation of *F. tularensis* subsp. *tularensis* a select agent by the Centers for Disease Control and Prevention (CDC), especially considering the historical development of *F. tularensis* bioweapons by several countries during the Cold War (13).

Within the lung, *F. tularensis* travels to the alveoli, where it infects a wide range of cell types, including alveolar macrophages, neutrophils, dendritic cells, monocytes, and alveolar type II epithelial cells (2, 18, 19). *F. tularensis* is taken up by host cells via looping phagocytosis, and after internalization, the bacteria escape the phagosome to replicate to high numbers in the cytoplasm (10, 11). In addition to the ability to replicate intracellularly, *F. tularensis* has the ability to suppress the proinflammatory immune response (2, 3, 8, 22, 40, 41). Several *F. tularensis* proteins have

been reported as virulence factors that are required for this intracellular life cycle; however, many of the identified virulence factors have little or no similarity to known proteins of other bacteria and their functions remain, for the most part, unknown.

Previously we identified a locus called *ripA* that is required for *F. tularensis* virulence. More specifically, deletion of this locus in the live vaccine strain (LVS) resulted in a mutant (LVSΔ*ripA*) that escapes the phagosome but is defective for intracellular replication (17) and fails to suppress the proinflammatory immune response (22). Not surprisingly, LVSΔ*ripA* is also attenuated in a pulmonary mouse model of tularemia (17). Deletion of *ripA* in the highly virulent strain *F. tularensis* Schu S4 results in a mutant that is defective for intracellular replication and attenuated in a mouse model as well, suggesting that RipA is required for virulence in highly pathogenic *F. tularensis* subsp. *tularensis* (our unpublished results).

RipA is a cytoplasmic membrane protein that is conserved among *Francisella* species (17). Interestingly, bioinformatic analyses show that there is sporadic representation of RipA-like proteins among prokaryotes, where RipA-like proteins are found in only specific strains of a given bacterial species. Similar to RipA, these other proteins are annotated as hypothetical proteins with no known functions or conserved domains; thus, the function of RipA remains unknown. RipA is a small protein (17 kDa) with three putative transmembrane domains and has a single cysteine found within the second membrane-spanning domain, which are unusual properties for a membrane protein, and examples of sim-

ilar proteins in the literature are sparse. The unusual biochemical properties of RipA, combined with its random distribution but obvious conservation within prokaryotes, led us to study RipA for its potential to provide insight into what may be a novel class of proteins and/or to reveal a novel virulence mechanism employed by *F. tularensis*.

In this study, we addressed the question of RipA function by analyzing RipA at the biochemical and molecular levels. Our results confirm a predicted topology model of RipA in the cytoplasmic membrane and show that RipA forms homooligomers. Using the topology model and alignments with other RipA-like proteins, we generated amino acid substitutions at conserved amino acids and deleted the two individual cytoplasmic domains within RipA. We analyzed these amino acid substitution and domain deletion mutants for the abilities to replicate intracellularly, suppress the immune response, and form RipA oligomers. We also identified and analyzed an intragenic suppressor mutant. Using the suppressor mutant as well as the substitution and deletion mutants of RipA, we showed that both cytoplasmic domains and at least four amino acids are required for RipA function.

MATERIALS AND METHODS

Bacterial strains. *F. tularensis* subsp. *holarctica* LVS was obtained from the CDC, Atlanta, GA. All *Francisella* strains were maintained on chocolate agar supplemented with 1% IsoVitaleX (BD) and, when applicable, 10 μg ml^{-1} kanamycin (Kan10) for selection. For growth of bacteria for infection or monitoring of *in vitro* growth, strains were propagated in Chamberlain's defined medium (CDM) (7). *Escherichia coli* TOP10 (Invitrogen) or DH10b (Invitrogen) was used for cloning. *E. coli* CC118 or BL21(DE3)pLysS was used for the expression of topology fusion reporter proteins. *E. coli* was propagated in Luria broth (LB) supplemented with ampicillin at 100 μg ml^{-1} (Amp100) or kanamycin at 50 μg ml^{-1} (Kan50), as necessary for antibiotic selection. All cultures were grown at 37°C with aeration.

Cell culture. TC-1 (ATCC CRL-2785) cells are a tumor cell line derived from mouse primary lung epithelial cells and were cultured in RPMI 1640 medium supplemented with 10% fetal bovine serum, 2 mM L-glutamine, 1.5 g liter^{-1} sodium bicarbonate, 10 mM HEPES, and 0.1 mM nonessential amino acids. J774A.1 (ATCC TIB-67) cells are a macrophage-like cell line derived from mouse sarcoma reticulum cells and were cultured in Dulbecco's minimal essential medium with 4.5 g liter^{-1} glucose, 10% fetal bovine serum, and 2 mM L-glutamine. Bone marrow-derived macrophages (BMMs) were generated by flushing C57BL/6 mouse femurs, and recovered cells were incubated for 6 days on 15-cm^2 non-tissue-culture-treated dishes in L929 cell-conditioned Dulbecco's modified Eagle's medium (DMEM). Nonadherent cells were removed by washing with phosphate-buffered saline (PBS), and BMMs were recovered from the dishes using 10 mM EDTA in PBS. For experiments, BMMs were maintained in DMEM plus 10% FBS.

Molecular techniques and mutagenesis. To generate constructs for RipA fusion protein expression using the Phusion polymerase (New England Biosciences), we PCR amplified *ripA* from LVS genomic DNA using primers that introduced XhoI and BamHI restriction sites directly before the start codon and in place of the stop codon of *ripA*, respectively. For cloning of truncated *ripA* constructs, the reverse primer introduced a BamHI restriction site at the respective locations in the *ripA* sequence but used the same forward primer. These constructs were first cloned into the pCR-Blunt II TOPO vector (Invitrogen) and subsequently subcloned using BamHI and XhoI restriction digestion and ligation into pWaldo-TEV-GFPe and pHA-4 (33) to generate the fusion protein expression constructs. For expression of fusion proteins, the plasmids were transformed into *E. coli* CC118 (pHA-4) or *E. coli* BL21(DE3)pLysS (pGFPe) by electroporation with selection on ampicillin at 100 μg ml^{-1} (pHA-4) or kanamycin at 50 μg ml^{-1} (pGFPe).

The cytoplasmic loop deletions in *ripA* were generated by gene synthesis of *ripA* containing the designated nucleotide deletions (corresponding to amino acids 4 to 47 or 105 to 151) and linker sequence insertion while maintaining the integrity of the flanking regions (Blue Heron). Each construct was PCR amplified from the synthesis vector and cloned into the pCR-Blunt II TOPO vector (Invitrogen), verified by DNA sequence analysis, and subsequently subcloned into pMP590 (*sacB* Kan^r) using the BamHI and NotI restriction sites (27). For allelic exchange, plasmids were electroporated into LVS and integrants were selected on chocolate agar containing kanamycin (10 μg ml^{-1}). Kan^r strains were grown overnight and plated on 10% sucrose for counterselection (loss of plasmid) (17). Deletions were confirmed by PCR analysis of genomic DNA using primers external to the deleted regions. The strategy for generation of the *ripA* deletion in LVS and for complementation of the *ripA* deletion has been described previously (17).

Single amino acid changes in RipA were generated by introducing 1- or 2-bp changes into the respective codon of the *ripA* DNA sequence using a QuikChange II site-directed mutagenesis kit (Stratagene) and following the manufacturer's protocol. The plasmid used for mutagenesis was the multicopy *Francisella* shuttle vector pKKMCS, which expressed *ripA* under the control of its native promoter and containing both 5′ and 3′ flanking regions. After DNA sequence confirmation of the mutations within *ripA*, the plasmids were each transformed into the LVSΔ*ripA* strain by electroporation and selection on chocolate agar with Kan10.

To generate hemagglutinin (HA)-tagged *ripA*, a fusion construct was made by splice overlap extension PCR (21) with primers that introduced the HA tag in frame into the C terminus of the coding sequence of *ripA* and including a glycine linker sequence between the end of the coding sequence and the HA tag. This construct was sequenced before use, cloned into the pMP590 suicide vector, and then used for allelic exchange to generate a chromosomally expressed, HA-tagged protein. Clones were screened using one primer specific to the tag and the second specific to a sequence on the chromosome. Additionally, this same construct was cloned into pKKMCS to generate a plasmid-expressed, HA-tagged protein. The integrity of the sequence was confirmed by DNA sequence analysis.

Green fluorescent protein (GFP) fluorescence and alkaline phosphatase activity assays. Procedures for protein expression, GFP fluorescence, and PhoA activity were adapted from previously published protocols (12, 15, 33). For the expression of GFP fusion proteins, *E. coli* BL21(DE3)pLysS containing each construct was grown in 1 ml LB–Kan50 overnight at 37°C and then diluted 1:50 into 500 μl LB–Kan50 per well of a 48-well plate and grown at 37°C and 250 rpm to an optical density at 600 nm (OD$_{600}$) of 0.3 to 0.4. Expression was then induced by the addition of 0.4 mM isopropyl-β-D-thiogalactopyranoside (IPTG), and cultures were grown to a final OD$_{600}$ of 0.6 to 0.8. Cell pellets were resuspended in 200 μl of buffer containing 50 mM Tris-HCl (pH 8.0), 200 mM NaCl, and 15 mM EDTA and incubated for 30 min at room temperature. Samples were then transferred to a black 96-well plate (Nunclone) and analyzed for GFP fluorescence using a 485-nm excitation filter, a 512-nm emission filter, and a cutoff of 495 nm with the TECAN Infinite M200 and analyzed using Magellan v6 software. For calculated GFP fluorescence, after subtraction of the cell background fluorescence, GFP emission was normalized against the OD$_{600}$ of the culture.

For expression of the PhoA fusion proteins, *E. coli* CC118 with each construct was grown in 1 ml LB–Amp100 overnight at 37°C and then diluted 1:50 into 500 μl LB–Amp100 per well of a 48-well plate and grown at 37°C and 250 rpm to an OD$_{600}$ of 0.13 to 0.18. Arabinose was added to a final concentration of 0.2%, and bacteria were grown to an OD$_{600}$ of 0.3 to 0.6. To prevent spontaneous PhoA activation, 1 mM iodoacetamide was added 10 min prior to harvesting and to all subsequent buffers. Samples were washed once in cold 10 mM Tris-HCl, pH 8.0, containing 10 mM MgSO$_4$ and resuspended in 1 ml cold 1 M Tris-HCl, pH 8.0. Then, 100 μl of each sample was added to 900 μl of 1 M Tris-HCl, pH 8.0, containing 1 mM ZnCl$_2$ and an OD$_{600}$ measurement of the remaining

sample was made. We next added 50 μl of 0.1% SDS and 50 μl of chloroform, vortexed the mixture for 15 s, incubated it at 37°C for 5 min to permeabilize the cells, and then placed the mixture on ice for 5 min to cool it. Finally, we added 100 μl of 0.4% p-nitrophenylphosphate (in 1 M Tris-HCl, pH 8.0) and incubated the mixture at 37°C. The tubes were monitored until each turned pale yellow, and then 120 μl of 1:5 0.5 M EDTA, pH 8.0, containing 1 M KH_2PO_4 was added to stop the reaction. The OD_{550} and OD_{420} of each sample were determined, and to calculate the activity, the following equation was used: Units of activity = $\{[OD_{420} - (1.75 \times OD_{550})] \times 1,000\}/$(time in minutes $\times OD_{600} \times$ volume of cells in milliliters).

Protein cross-linking. Overnight cultures of LVS were grown in CDM (pH 6.3) and either used for cross-linking or reseeded to grow to mid-log phase (150 Klett units). Each culture was aliquoted into 250- to 500-μl samples, washed once in 1$\times$ PBS, and then resuspended in the same buffer. Cross-linker was added to samples at a final concentration of 0.5% for formaldehyde or 0.5 mM for dithiobis(succinimidyl propionate) (DSP). Samples were incubated at room temperature for 30 min. For DSP-treated samples, 100 mM Tris-HCl (pH 7.4) was added to quench the reaction. All formaldehyde-treated samples were then washed once in ice-cold 1$\times$ PBS and resuspended in 200 μl SDS-PAGE loading buffer plus β-mercaptoethanol (βME) and heated at 60°C for 10 min (to maintain cross-linking) or at 100°C for at least 20 min (to cleave cross-linking). All DSP-treated samples were resuspended in SDS-PAGE buffer without βME (to maintain cross-linking) or with βME (to cleave cross-linking) and heated at 100°C for 10 min. All samples were analyzed by SDS-PAGE and Western blot assay as described below.

Membrane fractionations. LVS was grown overnight in 15-ml cultures in CDM (pH 6.3) at 37°C, pelleted, and washed once in lysis buffer (150 mM NaCl, 10 mM Tris, pH 7.5). Cells were lysed in Lysis Matrix B tubes (MP Biomedicals) by beating in a Mini-BeadBeater (Biospec Products) for 45 s twice at 4°C. Cell lysates were collected after the beads settled and clarified by centrifugation at 12,000 $\times$ g for 3 min. Crude membrane fractions were separated from cytoplasmic fractions by ultracentrifugation at 100,000 $\times$ g for 90 min, with the cytoplasmic fraction being in the supernatant. The remaining crude membrane fraction pellet was solubilized in lysis buffer containing a final concentration of 0.5% Sarkosyl and incubated at room temperature with shaking for 30 min. Insoluble outer membrane components were isolated from the cytoplasmic membrane fractions (supernatant) by centrifugation at 100,000 $\times$ g for 60 min (17). Protein concentrations in each fraction were determined using a standard bicinchoninic acid (BCA) assay (Thermo Scientific).

SDS-PAGE and Western blot assay. Either 4 to 20% or 12% Pierce Precise protein gels (Thermo Scientific) were loaded with the designated samples at equal concentrations as determined by BCA assay and run using BupH Tris-HEPES-SDS running buffer at 120 V. To determine molecular masses, either Benchmark Prestained Protein Ladder (Invitrogen) or PageRuler Plus Prestained Ladder (Fermentas) was used. For Western blot assay, gels were transferred to nitrocellulose membranes at 400 mA for 45 min and then blocked overnight in 1% bovine serum albumin in PBS–Tween 20 (PBST). All antibodies were incubated at room temperature with rocking for 1 h with PBST washes between incubations. The primary antibody used was a rabbit anti-RipAaa1-19, anti-RipAaa112-128 (both described below), or mouse anti-HA monoclonal antibody (Sigma), and the secondary antibody used was a goat anti-rabbit IgG IRDye 680 or goat anti-mouse IgG IRDye 800CW antibody. Protein was detected by near infrared fluorescence at 700 nm or 800 nm using the Odyssey Infrared Imaging System (LI-COR Biosciences).

Generation of affinity-purified antibodies against RipA peptides. Two RipA peptide sequences corresponding to amino acids 1 to 19 and amino acids 112 to 128 were synthesized by YenZyme Antibodies, LLC, for the production of each peptide and then rabbit antiserum and affinity purification of antibodies against each peptide. Preimmune sera were also collected from the rabbits and used during initial tests of the antibodies for reactivity and specificity in Western blot assays of LVS lysates.

Gentamicin protection assays. TC-1 epithelial cells or J774A.1 macrophages were inoculated with LVS at a multiplicity of infection (MOI) of 100 after determination of bacterial concentrations in Klett units. All LVS strains were grown overnight in CDM (pH 6.3) prior to inoculation. The cells were incubated with the bacterial inoculum for 2 h (J774A.1) or 4 h (TC-1) and then incubated with medium containing 25 μg ml^{-1} gentamicin for an additional 2 h to kill the extracellular bacteria. At 4 h (J774A.1) or 6 h (TC-1) postinfection and at 24 h postinfection, medium was removed, cells were washed with PBS and then scraped from the dish, and the bacteria were serially diluted and plated to determine the number of viable bacteria.

IL-1β enzyme-linked immunosorbent assays (ELISAs). BMMs were prepared as described above and seeded into 12-well dishes at 1×10^6/well on the day of infection. At 1 to 2 h after plating, cells were inoculated with bacteria at an MOI of 500 and incubated at 37°C. After 24 h, the supernatants from each well were collected and centrifuged to pellet cellular debris. The IL-1β ELISA was performed using the BD OptEIA mouse IL-1β ELISA kit (BD Biosciences) according to the manufacturer's protocol. The OD_{450} was read using a TECAN Infinite M200 and analyzed using Magellan v6 software.

Statistical analysis. For intracellular replication assay data, the differences in total CFU values at the 24-h time point for each strain were analyzed for significance using the unpaired, two-tailed Student t test. For IL-1β ELISA data, significance was determined by repeated-measures one-way analysis of variance with a Dunnett multiple-comparison posttest. Other details and P values are included in the figure legends. All statistical values were calculated using GraphPad Prism v.5 software (GraphPad).

RESULTS

Mapping of RipA topology using carboxyl-terminal fusion reporter proteins. RipA is a 179-amino-acid cytoplasmic membrane protein estimated to be approximately 17 kDa (17). Using the annotated amino acid sequence for RipA and the TMHMM software (38), the topology of RipA was predicted. The TMHMM-predicted RipA topology was also supported using several other prediction programs (data not shown). The data output from TMHMM was used in TMRPres2D (39) to generate the image depicted in Fig. 1A. This model predicted that RipA has three membrane-spanning domains (amino acids 51 to 71, 83 to 103, and 152 to 172), with the amino terminus (N terminus) in the cytoplasm and the carboxyl terminus (C terminus) in the periplasm. Also predicted within RipA are two large cytoplasmic domains (amino acids 1 to 50 and 104 to 151) and two smaller periplasmic domains (amino acids 72 to 82 and 173 to 179). It is rare for a protein to have only three transmembrane domains with this orientation, and very few such proteins have been thoroughly characterized (12, 15, 33).

Considering the value of validating such a unique topology for RipA, we made use of a fusion reporter protein system that has been used to map *E. coli* cytoplasmic membrane proteins (12, 15, 33). In this system, either GFP or alkaline phosphatase (PhoA) was fused at the C-terminal end of recombinant proteins or peptides and expressed in *E. coli*, and GFP fluorescence or PhoA activity was assayed. GFP is only fluorescent in the cytoplasm, and PhoA is active only in the oxidizing environment of the periplasm (14). Thus, by fusing GFP or PhoA to a protein, one can determine the cytoplasmic or periplasmic location of the C terminus of the protein. GFP or PhoA was fused at the C terminus of RipA and at four locations predicted to be near transmembrane junctions of RipA, thereby generating fusion proteins expressing amino acids 1 to 47, 1 to 80, 1 to 106, 1 to 148, and also 1 to 179 (full-length RipA). The
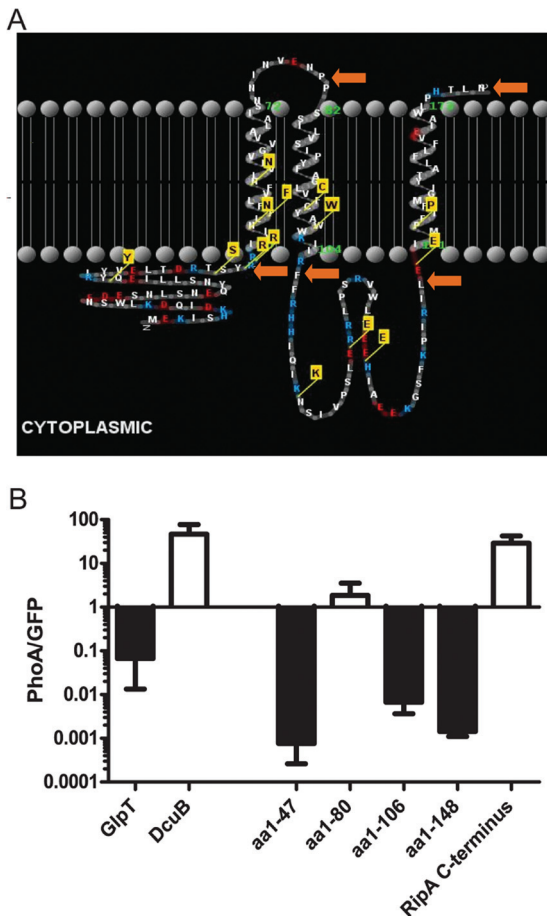
A

B

FIG 1 Mapping of RipA within the cytoplasmic membrane using C-terminal fusion reporter proteins in *E. coli*. (A) The predicted topology model of RipA was determined using TMHMM, and the image was made using TMRPres2D. The yellow tags label the 13 amino acids that are conserved among RipA-like proteins in other bacterial strains, as well as the single cysteine found within *Francisella* RipA. The orange arrows highlight the amino acids at which the fusion reporter proteins were made. The colors designate electrostatic potential, with red highlighting negatively charged amino acids and blue highlighting positively charged amino acids. (B) RipA C-terminal fusion proteins were expressed in *E. coli* alongside GlpT and DcuB C-terminal fusion proteins as GFP- and PhoA-positive controls, respectively. Each strain was assayed for PhoA activity or GFP fluorescence, as appropriate. Data are represented as PhoA-to-GFP ratios consolidated from at least three experiments for each construct performed in duplicate or triplicate. Error bars represent the standard deviations of the composite PhoA-to-GFP ratios from all experiments. Primary expression data are presented in Table S2 in the supplemental material.

locations on RipA at which the fusions were made are highlighted in Fig. 1A by the orange arrows. C-terminal fusion proteins of DcuB and GlpT, two *E. coli* proteins that have been identified as having C termini with periplasmic and cytoplasmic locations, respectively, were included as controls (12). The GFP fusion proteins were expressed in *E. coli* BL21(DE3)pLysS, and PhoA fusion proteins were expressed in *phoA* mutant *E. coli* CC118. The GFP fluorescence or PhoA activity of each construct was measured and graphed as the ratio of PhoA to GFP (Fig. 1B). As expected, the control DcuB fusion protein had a high PhoA-to-GFP ratio, corresponding to a periplasmic location, and the control GlpT fusion protein had a low PhoA-to-GFP ratio, corresponding to a cyto-

plasmic location. In terms of RipA, fusion proteins for amino acids 1 to 47, 1 to 106, and 1 to 148 had low PhoA-to-GFP ratios (i.e., high GFP fluorescence), corresponding to a cytoplasmic location for RipA at amino acids 47, 106, and 148. Constructs for amino acids 1 to 80 and 1 to 179 had higher PhoA-to-GFP ratios (i.e., high PhoA activity), corresponding to a periplasmic location at amino acids 80 and 179. Thus, the fusion protein reporter system supports the idea that the predicted RipA topology is correct.

RipA forms homoligomers, as revealed by *in vivo* cross-linking in LVS. It is possible that RipA, as a small, integral cytoplasmic membrane protein, interacts with itself and/or other proteins. Additionally, under nonreducing conditions, higher-molecular-mass bands have been observed on Western blots probed with anti-RipAaa1-19 antibody. For example (Fig. 2A), under nonreducing conditions (i.e., no addition of βME), there are at least three higher-molecular-mass bands, whereas there is only one higher-molecular-mass band under reducing conditions. This result hints that RipA may be interacting with itself as a homoligomer. In order to capture potential RipA oligomerization *in vivo*, two different bifunctional, reversible chemical cross-linkers, formaldehyde and DSP, were used to treat LVS grown in chemically defined medium. Formaldehyde was added to cells at concentrations ranging from 0.1 to 1%, and the optimal concentration was found to be 0.5%, which was used for subsequent experiments. Cleavage of formaldehyde-mediated protein interactions is accomplished by boiling samples. DSP was added to cells at concentrations ranging from 0.5 to 1 mM, and the optimal concentration was found to be 0.5 mM, which was used for subsequent experiments. DSP-mediated interactions are reversed by the addition of βME. Cross-linking with either formaldehyde or DSP revealed that RipA formed two to four higher-molecular-mass bands of 40 kDa, 55 kDa, 70 kDa, and sometimes 100 kDa that disappeared upon cleavage of the cross-linker (Fig. 2B). These higher-molecular-mass bands likely represent a range of oligomeric states of RipA.

To determine whether the higher-molecular-mass complexes correspond to RipA interacting with itself, as opposed to other proteins, cross-linking experiments were performed with two complementary strains: HA-tagged *ripA* expressed on a plasmid in wild-type LVS and chromosomally expressed HA-tagged *ripA* with wild-type *ripA* on a plasmid. With each strain, both the native and HA-tagged RipA proteins were expressed by the *ripA* promoter on the same multicopy plasmid backbone. Each of these strains, as well as wild-type LVS, was cross-linked with formaldehyde and analyzed via Western blot assay using antibodies against both RipAaa1-19 and the HA tag. Secondary antibodies conjugated to different-wavelength infrared dyes allowed for differential labeling of native and HA-tagged RipA (RipA-HA), and the HA tag allowed for differentiation by size. Due to the lower resolution of the higher-molecular-mass bands, we focused on the ~40-kDa band that corresponded to a potential RipA dimer. As expected, in place of a single band, there were three bands differing by only a few kDa in the two strains containing HA-tagged and wild-type *ripA*. The lowest-molecular-mass band corresponds to RipA/RipA dimers, the middle-molecular-mass band corresponds to RipA/RipA-HA dimers, and the highest-molecular-mass band corresponds to RipA-HA/RipA-HA dimers (Fig. 2C). These data suggest that RipA interacts with itself and forms a homodimer and possibly higher-number homoligomers. Work to identify whether RipA also interacts with other proteins is under way.
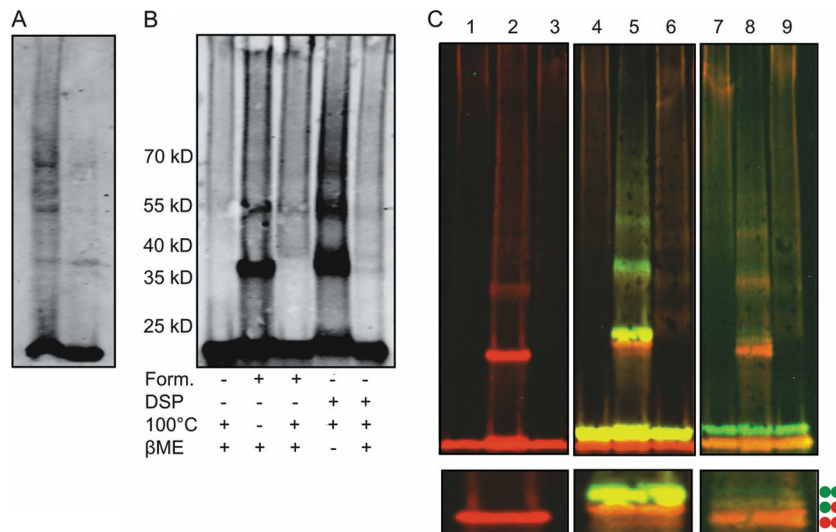
FIG 2 *In vivo* protein cross-linking of RipA. (A) Western blot assay of LVS lysates probed with anti-RipAaa1-19 antibody after SDS-PAGE under nonreducing conditions (no βME; left lane) and under reducing conditions (right lane). (B) LVS treatment with either 0.5 mM DSP or 0.5% formaldehyde (Form.) and analysis by Western blot assay using anti-RipAaa1-19 antibody. Incubation of samples at 100°C (formaldehyde) or addition of βME (DSP) cleaved selected samples, as shown at the bottom. (C) LVS (lanes 1 to 3), LVS with plasmid-expressed RipA-HA (lanes 4 to 6), and LVS with chromosomally expressed RipA-HA plus plasmid-expressed wild-type RipA (lanes 7 to 9) were grown overnight, incubated with 0.5% formaldehyde, and analyzed by Western blot assay probed with anti-RipAaa1-19 (red) and anti-HA (green) antibodies. Lanes: 1, 4, and 7, untreated; 2, 5, and 8, 0.5% formaldehyde; 3, 6, and 9, 0.5% formaldehyde plus 100°C. The images below each panel of the Western blot are cropped and enlarged from the Western blot to focus on the bands of interest. Although from the same blot, the panel containing lanes 7 to 9 was exposed at a lower intensity in the red channel in order to distinguish the fainter upper band (green channel), and this results in the upper band appearing more green than the expected yellow, as shown in lanes 4 to 6. All of the data shown are representative of at least three experiments.

The cytoplasmic domains of RipA are important for RipA function. Having determined the topology of RipA in the cytoplasmic membrane, we set out to identify which domains of RipA are required for function. Since protein-protein interactions often occur in the cytoplasm and because there are two large domains within RipA in the cytoplasm, the two cytoplasmic domains were targeted for analysis as putative functional domains using intracellular replication, induction of IL-1β secretion by infected macrophages, and RipA oligomer formation as functional readouts. Independent deletion of the domain corresponding to amino acids 4 to 47 or 105 to 151 was constructed by replacement with a 15-amino-acid linker sequence rich in glycines and serines and also two prolines for flexibility. This resulted in two LVS mutants designated LVS *ripA*Δaa4-47 and LVS *ripA*Δaa105-151. These mutants were analyzed for intracellular replication in J774A.1 murine macrophages (Fig. 3A) and TC-1 epithelial cells (Fig. 3B). The results demonstrate that LVS *ripA*Δaa4-47 and LVS *ripA*Δaa105-151 are both defective for intracellular replication in each cell type, similar to LVSΔ*ripA*. Each mutant was also tested for the ability to induce IL-1β secretion, as measured by ELISA in supernatants from infected BMMs (Fig. 3C). Similar to what was seen with LVSΔ*ripA*, LVS *ripA*Δaa4-47 and LVS *ripA*Δaa105-151 both induced increased levels of IL-1β in infected BMMs. To verify that each protein was expressed in the proper location, cytoplasmic membrane fractions of each mutant were analyzed via Western blot assay using antibodies against RipAaa1-19 or RipAaa112-128 (Fig. 3D). Deletion of amino acids 4 to 47 and 105 to 151 resulted in RipA proteins that are expressed in the correct location, though at a slightly lower level. It is unlikely that the reduced amount of membrane-associated protein was solely responsible for the mutant phenotypes since we found no direct correlation between RipA protein expression levels and intracellular growth (see Fig. S1 in the supplemental material). Finally, to determine the role of each domain in the ability of RipA to oligomerize, we performed *in vivo* cross-linking with formaldehyde or DSP as described above, excluding the first deletion mutant, whose protein expression was too low to detect any cross-linking (Fig. 3E). Unlike LVS, which again displayed several higher-molecular-mass complexes, no RipA oligomer formation was observed for LVS *ripA*Δaa105-151, suggesting that the second cytoplasmic domain is required for binding. Together, these data suggest that both cytoplasmic domains, corresponding to amino acids 4 to 47 and 105 to 151, are required for RipA function and that at least the second cytoplasmic domain is required for RipA oligomerization.

At least four amino acids within RipA are required for intracellular replication and suppression of the proinflammatory response. Analysis of the results from a BLASTp search using the protein sequence of RipA revealed a relatively short list of RipA-like proteins that have E values below zero. Moreover, these proteins are found only in individual strains of a given species, which seem to be randomly distributed across prokaryotes (see Table S1 in the supplemental material). Thirteen amino acids are identical or highly conserved among the 15 RipA-like proteins with E values of less than 10^{-3}. As an additional approach to identifying regions required for RipA function, mutants expressing alanine substitutions were made at each of these 13 conserved amino acids found among the RipA-like proteins discussed above, as well as the single cysteine, totaling 14 amino acid substitution mutants. Site-directed mutagenesis was performed on a plasmid containing *ripA*, and the mutated plasmid was transformed into LVSΔ*ripA*. Each mutant was screened for expression of RipA in the cytoplas-
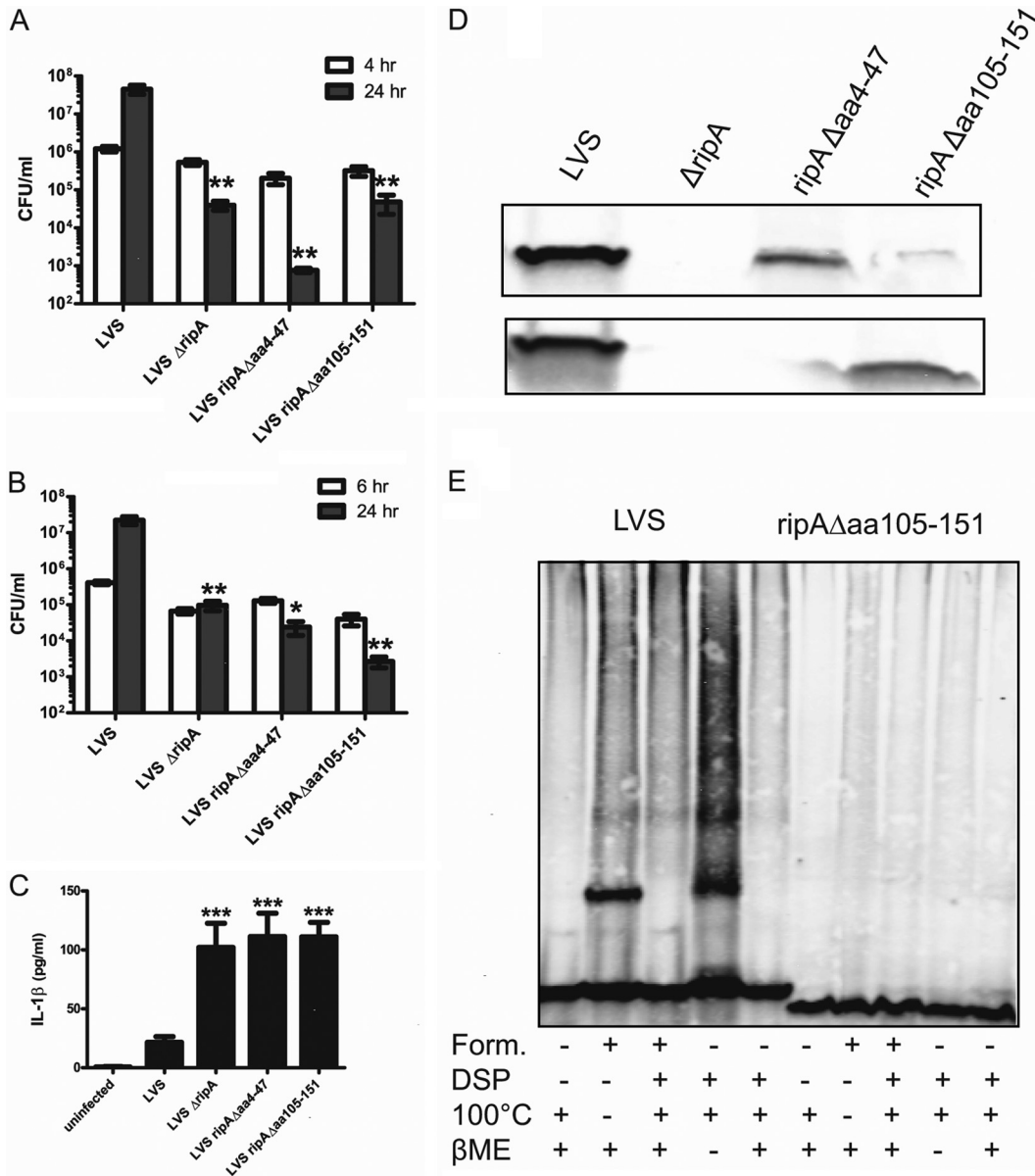
FIG 3 Characterization of two RipA cytoplasmic domain deletion mutants. (A) Intracellular replication of wild-type LVS, LVSΔ*ripA*, LVS *ripA*Δaa4-47, and LVS *ripA*Δaa105-151 was assessed within J774A.1 macrophages (A) and TC-1 epithelial cells (B) by gentamicin protection assay. Each graph is representative of one of three experiments, each performed in triplicate, and the error bars show the standard deviations of triplicates. (C) Secretion of IL-1β by BMMs at 24 h measured by ELISA in supernatants of cells left untreated or incubated with LVS, LVSΔ*ripA*, LVS *ripA*Δaa4-47, or LVS *ripA*Δaa105-151. The graph shows the results of one of at least three experiments performed in triplicate, with error bars representing the standard deviations of replicates. (D) Protein expression of LVS, LVSΔ*ripA*, LVS *ripA*Δaa4-47, and LVS *ripA*Δaa105-151 in LVS cytoplasmic membrane fractions was determined by Western blot assay probed with anti-RipAaa112-128 for LVS *ripA*Δaa4-47 (top) or anti-RipAaa1-19 antibody for LVS *ripA*Δaa105-151 (bottom). (E) *In vivo* cross-linking on wild-type LVS (lanes 1 to 5) and LVS *ripA*Δaa105-151 (lanes 6 to 10) was performed by treatment with 0.5% formaldehyde or 0.5 mM DSP. For some samples, cleavage was achieved by the addition of βME (DSP) or incubation at 100°C (formaldehyde [Form.]), as shown at the bottom. Cross-linking was followed by Western blot assay probed with anti-RipAaa1-19 antibody. The Western blots shown are representative of at least three experiments. Statistical significance was determined by comparing the values for each respective mutant to the values for LVS. *, $P < 0.05$; **, $P < 0.01$; ***, $P < 0.001$.

mic membrane using the anti-RipAaa1-19 antibody via Western blot assay of lysates of cytoplasmic membrane fractions (Fig. 4A). To determine whether any mutant could *trans* complement LVSΔ*ripA*, each strain was analyzed for the ability to replicate intracellularly in J774A.1 macrophages (Fig. 4B) or TC-1 epithelial cells (Fig. 4C) and for induction of IL-1β secretion by infected BMMs (Fig. 4D). The S46A, R48A, R49A, N53A, F55A, N60A,

C97A, and E134A mutants *trans* complemented LVSΔ*ripA* in all of the assays, suggesting that none of these residues are required for RipA function. Of the remaining mutants, the W100A and P154A mutants had variable or intermediate phenotypes; however, the Y35A, K114A, E122A, and E150A mutants did not *trans* complement LVSΔ*ripA* in any of the assays. Thus, at least these four respective amino acids, Y35, K114, E122, and E150, are re-
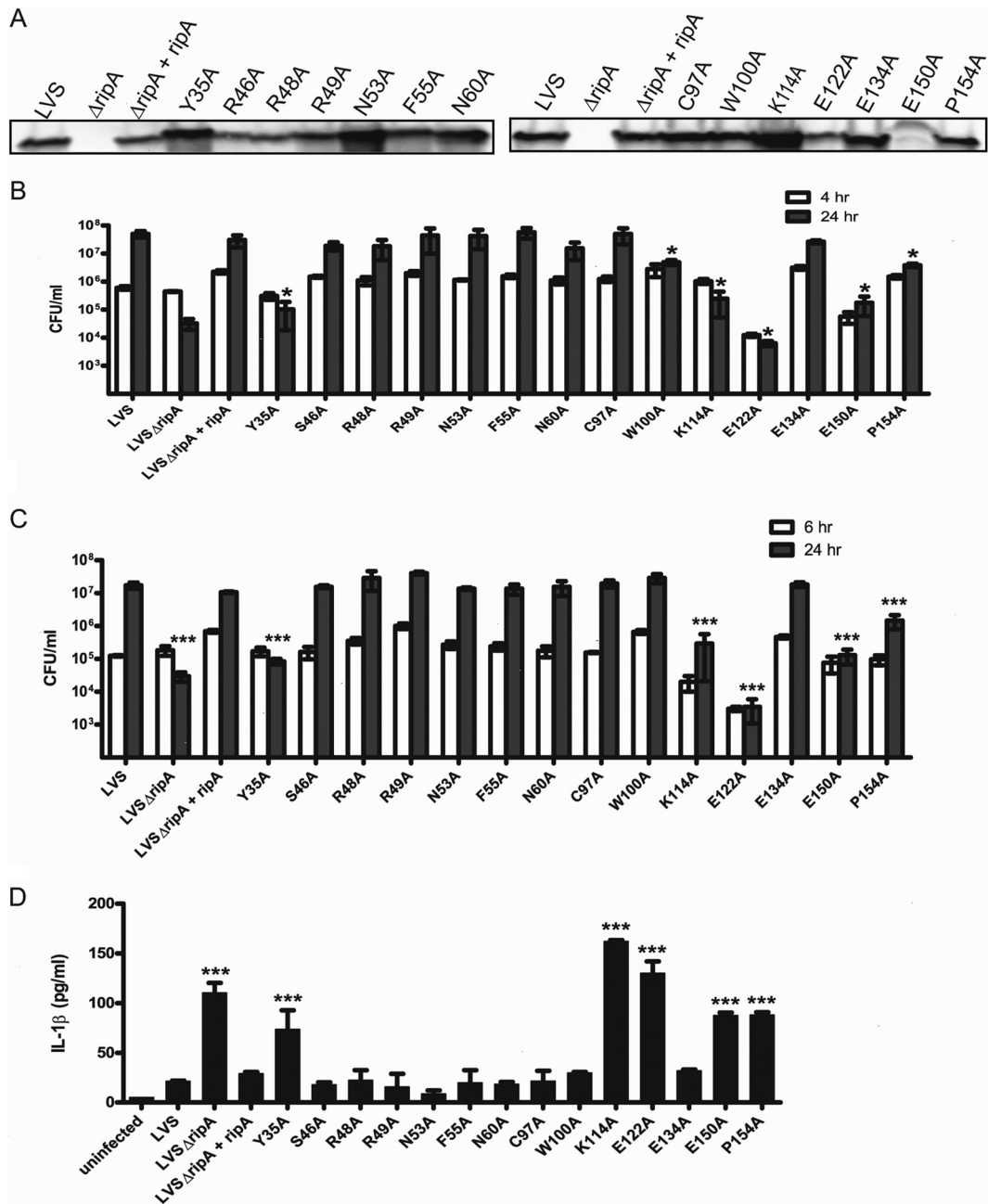
FIG 4 Characterization of RipA alanine substitution mutants for intracellular replication and suppression of the proinflammatory response. (A) The 14 RipA alanine substitution mutants were expressed in LVSΔ*ripA* and analyzed for protein expression in the cytoplasmic membrane fractions of LVS by Western blot assay probed with anti-RipAaa1-19 antibody. Each mutant was assessed for intracellular replication in J774A.1 macrophages (B) and TC-1 epithelial cells (C) by gentamicin protection assay. The graphs represent consolidated data for each mutant from a representative of at least two experiments performed in triplicate, and the error bars show the standard deviations of triplicates. (D) Each mutant was analyzed for induction of IL-1β secretion by infected BMMs at 24 h by ELISA. The graph represents consolidated data for each mutant from a representative of at least two experiments performed in duplicate or triplicate, and the error bars show standard deviations of replicates. Statistical significance was determined by comparing the values for each respective mutant to the values for LVSΔ*ripA* + *ripA* since this strain has the backbone plasmid on which the mutants were made. *, $P < 0.05$; ***, $P < 0.001$.

quired for RipA function, and this corroborates the finding obtained with the domain deletion mutants that both cytoplasmic domains are required for RipA function.

Conservative and charge reversal amino acid changes confirm a role for K114, E122, and E150 in RipA function. Due to their location in the second cytoplasmic domain and to further

investigate the importance of K114, E122, and E150 for RipA function, both conservative and charge reversal substitutions were made at each amino acid. The substitution mutations were again generated using site-directed mutagenesis, and the mutants were assessed for intracellular replication (Fig. 5A and B) and induction of IL-1β secretion (Fig. 5C). For conservative changes E122D and
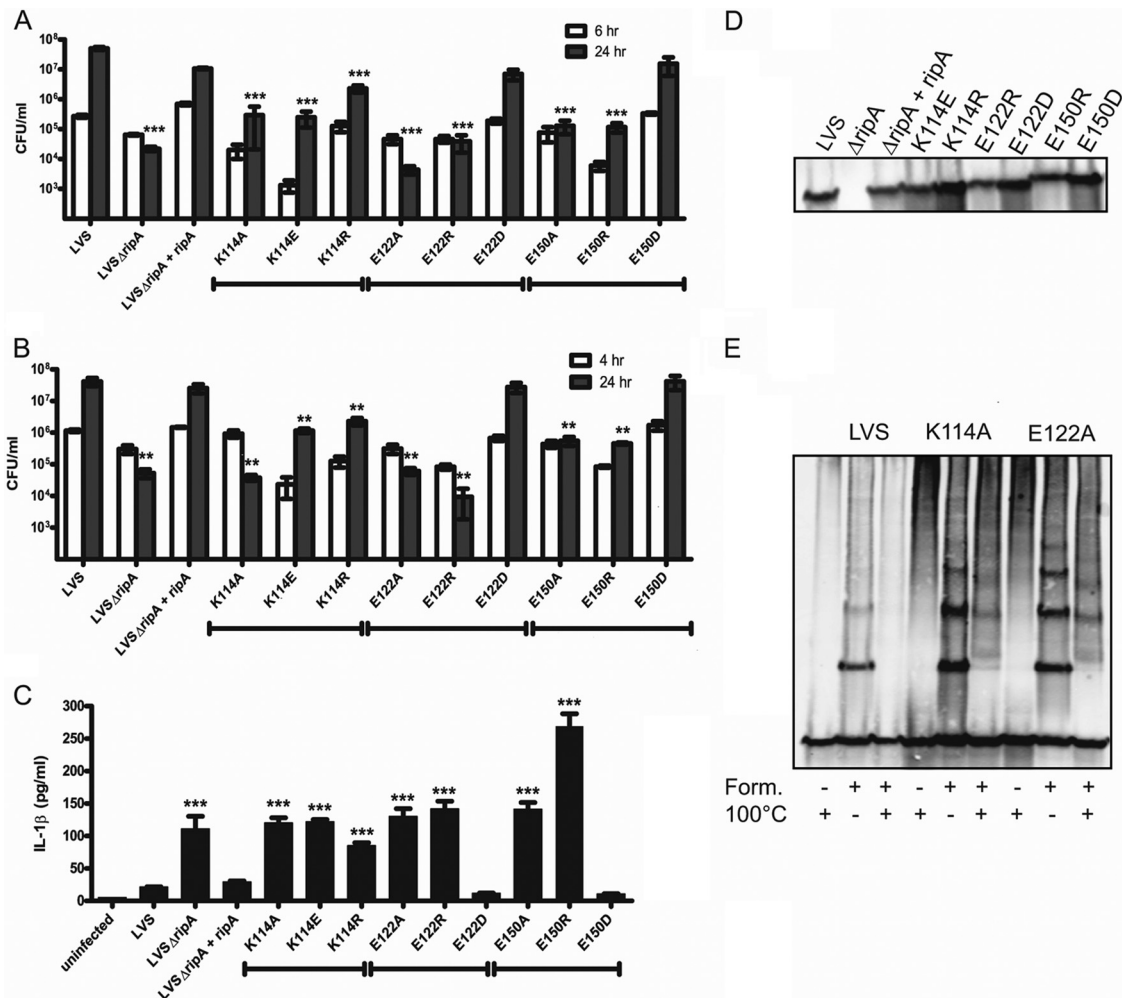
FIG 5 Further analysis of the importance of amino acids K114, E122, and E150 in RipA function. The charge reversal and conservative amino acid substitution mutants for K114, E122, and E150 were assessed for intracellular replication within TC-1 cells (A) and J774A.1 macrophages (B) by gentamicin protection assays. The graphs represent consolidated data for each mutant from a representative of at least two experiments performed in triplicate, and the error bars show standard deviations of triplicates. (C) Each mutant was analyzed for induction of IL-1β secretion by BMMs at 24 h by ELISA in supernatants of infected cells. The graph represents consolidated data for each mutant from a representative of at least two experiments performed in duplicate or triplicate, and the error bars show standard deviations of replicates. (D) Each mutant was assessed for protein expression in the cytoplasmic membrane fraction of LVS by Western blot analysis probed with anti-RipAaa1-19 antibody. (E) Wild-type LVS and the K114A and E122A mutants were cross-linked with 0.5% formaldehyde (Form.) and analyzed by Western blot assay probed with anti-RipAaa1-19 antibody. Statistical significance was determined by comparing values for each respective mutant to the values for LVS$\Delta ripA$ + *ripA*. **, $P < 0.01$; ***, $P < 0.001$.

E150D, each mutant *trans* complemented the LVS$\Delta ripA$ phenotype, whereas the respective charge reversal substitution E122R and E150R mutants did not. These data not only confirm a role for E122 and E150 in RipA function, they suggest that the charge at these sites is also important. With the conservative change K114R mutant, an intermediate phenotype, or partial *trans* complementation, was observed. With the charge reversal K114E mutant, no *trans* complementation was observed. Based on these data, we conclude that K114 is important for RipA function but cannot determine whether the charge is responsible for its function. To verify that each mutant was expressed in the cytoplasmic membrane, protein expression was determined via membrane fractionations and Western blot assay using anti-RipAaa1-19 antibody as described above (Fig. 5D). Lastly, cross-linking experiments were performed with the K114A, E122A, and E150A mutants to determine whether any of these amino acids is re-

quired for RipA oligomerization (Fig. 5E and 6D). Interestingly, each mutant was still able to form RipA oligomers, suggesting either that these amino acids are not involved in oligomerization or that there are multiple amino acids that mediating binding, such that changing one amino acid is not sufficient to eliminate the interaction.

Identification of an intragenic suppressor mutant supports a role for the first cytoplasmic domain in RipA function. During the course of experiments with the alanine substitution mutants, the plasmids from LVS were repeatedly sequenced to verify the integrity of the *ripA* sequence and the desired mutations within RipA. In this process for K114A, E122A, and E150A, we frequently observed mutations that resulted in a frameshift, loss of the alanine substitution mutation (rare), or single amino acid changes within *ripA*. Due to the relatively high frequency of mutations found within RipA-E150A, one of the single amino acid changes
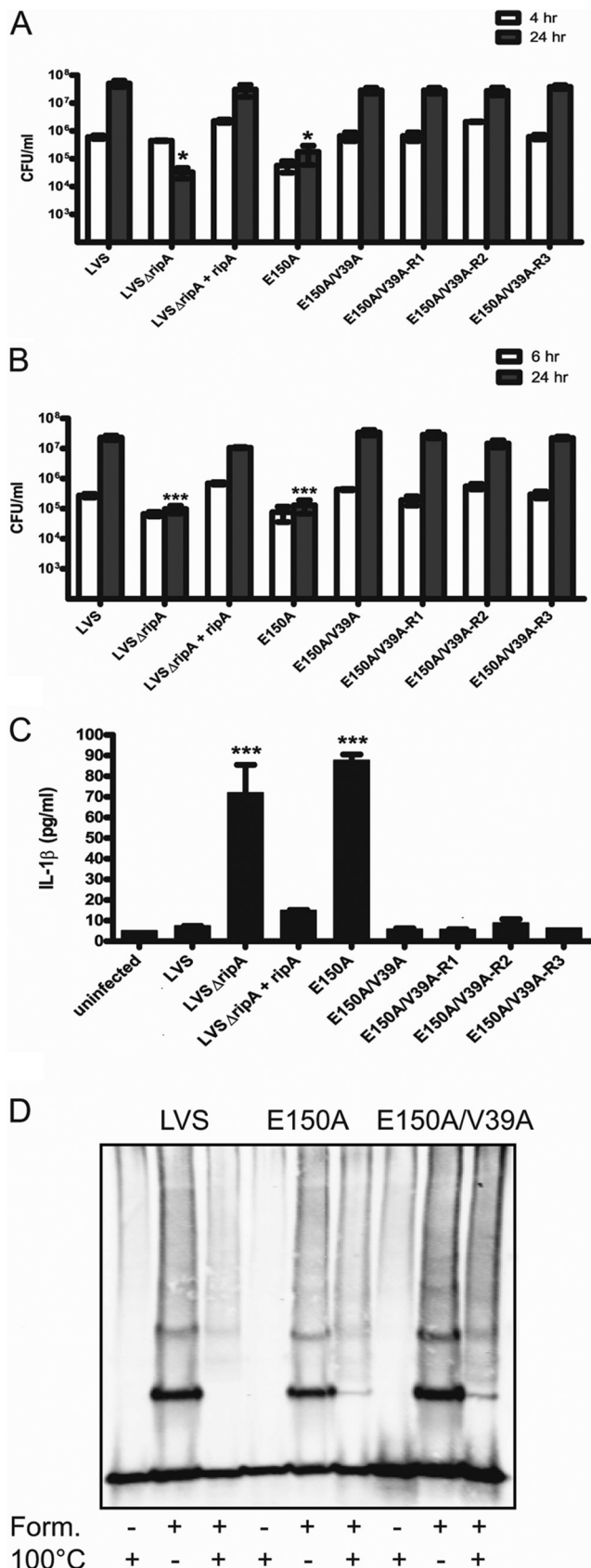
identified was selected for further characterization, i.e., E150A with an additional V39A change, which was designated E150A/V39A. Assays for intracellular replication (Fig. 6A and B) and also for IL-1β secretion (Fig. 6C) revealed that this mutant *trans* complemented LVSΔ*ripA*, suggesting that this new mutation was an intragenic suppressor. To confirm that the phenotype was the result of the intragenic mutation and not the result of an extragenic mutation, the plasmid containing RipA E150A/V39A was isolated and retransformed into LVSΔ*ripA* three independent times. Each of these new E150A/V39A transformants was assayed for intracellular replication and for IL-1β secretion and displayed the same phenotype as the original suppressor mutant, confirming that the V39A substitution was responsible for *trans* complementation. After formaldehyde cross-linking, the E150A/V39A mutant also displayed the same higher-molecular-mass bands as the wild type and the E150A mutant, suggesting that this *trans* complementation was not a result of altered oligomeric complex formation (Fig. 6D). Of note, a mutant containing only the V39A substitution in the LVSΔ*ripA* deletion background did not display a defect in intracellular replication (data not shown). Overall, when considering the intragenic suppressor data, one can infer that the two cytoplasmic domains may be interacting with each other or alternatively with another protein or molecule.

DISCUSSION

F. tularensis is a highly successful pathogen; however, many of the known virulence factors still have no identified function. RipA is a virulence factor that was previously shown to be required *in vivo* in a pulmonary mouse model of tularemia, likely in part due to its inability to suppress the proinflammatory response like wild-type *F. tularensis* LVS or Schu S4 (17, 22; unpublished observations). Furthermore, RipA is required for *F. tularensis* intracellular replication in both macrophages and epithelial cells (17). However, LVSΔ*ripA* escapes the phagosome with kinetics similar to those of wild-type *F. tularensis* (17). This phenotype suggests that a lack of RipA results in a strain unable to adapt to the environment of the host cell cytoplasm. Not surprisingly, LVSΔ*ripA* grows poorly *in vitro* at higher pHs and the expression of both the *ripA* transcript and the RipA protein is upregulated at higher pHs and between 1 and 6 h postinfection of host cells, all correlating with a role for RipA in adaptation to the cytoplasm (16).

This study addressed the question of RipA function at the biochemical and molecular levels. Preceding studies demonstrated

FIG 6 Identification and characterization of an intragenic suppressor mutation in RipA E150A. A spontaneous V39A suppressor mutation appeared in the E150A mutant (E150A/V39A), and this plasmid was used to retransform three LVSΔ*ripA* strains and generate E150A/V39A-R1, -R2, and -R3. Wild-type LVS, LVSΔ*ripA*, LVSΔ*ripA* + *ripA*, the E150A mutant, the E150A/V39A mutant, and the E150A/V39AR1-3 mutant were assessed for intracellular replication within J774A.1 macrophages (A) and TC-1 epithelial cells (B) by gentamicin protection assay. The graphs represent consolidated data for each mutant from a representative of at least two experiments performed in triplicate, and the error bars show standard deviations of triplicates. (C) Secretion of IL-1β by macrophages at 24 h as measured by ELISA in supernatants of infected cells. The graph shows a representative of at least two experiments performed in duplicate or triplicate, and the error bars show standard deviations of replicates. (D) Wild-type LVS, the E150A mutant, and the E150A/V39A mutant were cross-linked using 0.5% formaldehyde (Form.) and analyzed by Western blot assay probed with anti-RipAaa1-19 antibody. The Western blot shown is representative of at least two experiments. Statistical significance was determined by comparing the values for each respective mutant to the values for LVSΔ*ripA* + *ripA*. *, $P < 0.05$; ***, $P < 0.001$.

that RipA localizes to the cytoplasmic membrane of *F. tularensis* (17). Here, the topology of RipA within the cytoplasmic membrane was determined in terms of orientation and subcellular location of functional domains. RipA has three transmembrane domains, two large cytoplasmic domains, and two smaller periplasmic domains with the N terminus in the cytoplasm and the C terminus in the periplasm. Additionally, RipA was shown to form homoligomers in the membrane by using *in vivo* cross-linking with either formaldehyde or DSP, and even in the absence of protein cross-linkers, the protein can exist in higher-order forms. The first of several higher-molecular-mass bands appears to correspond to at least a dimer size (~40 kDa), suggesting that RipA forms a homodimer. RipA homodimerization was confirmed by experiments using strains expressing both RipA and RipA-HA where, in place of the single 40-kDa band, there were three bands corresponding to RipA-RipA dimers, RipA–RipA-HA dimers, and RipA-HA–RipA-HA dimers. Due to the lack of resolution of the higher-molecular-mass bands in these experiments and since these bands are not exactly trimer, tetramer, etc. in size, we cannot definitively say whether or not these bands are solely RipA or RipA cross-linked to another protein; however, based on the characteristic banding pattern, we suspect that these forms represent homoligomers as well. We are in the process of determining whether or not RipA interacts with any other *F. tularensis* proteins. Further insight into RipA topology, structure, and ultimately function could be gained by doing biochemical experiments such as size exclusion chromatography and solving the crystal structure.

Francisella RipA proteins and some of the other RipA-like proteins have only a single cysteine found in the second transmembrane domain, which is uncommon. The highly reactive thiol group of a cysteine is known to be involved in several biological functions, most prominently the formation of disulfide bonds with other cysteine residues. These disulfide bonds can occur within the same protein to maintain tertiary structure or with a cysteine from another protein to mediate intermolecular complex formation, making unpaired cysteines quite rare. Due to the high reactivity of the thiol group, cysteine is not usually found in isolation, and proteins with a single cysteine form oligomers or bind metals or other molecules via this amino acid. The facts that the RipA C97A mutant still formed oligomers (data not shown), was not attenuated for intracellular growth, and did not induce IL-1β secretion by infected macrophages suggest that this is not the case for RipA. Thus, the role of this single cysteine in RipA function remains unknown. One explanation is that there is no specific role for C97 in RipA function, especially considering that the cysteine is not completely conserved in all RipA-like proteins and that in some RipA-like proteins there is more than one cysteine present. Alternatively, the cysteine has a function unique to only *Francisella* RipA or a subset of RipA-like proteins. An interesting possibility is that the cysteine is involved in conformational changes in the RipA protein or binds to a small molecule, as opposed to directly binding to protein partners.

Employing the topology model of RipA, we targeted specific domains for assessment of their roles in RipA function. Using domain deletion mutants, we found that each cytoplasmic domain is required for RipA function in terms of intracellular replication in macrophages and epithelial cells and suppression of the proinflammatory immune response and that at least the second cytoplasmic domain is required for RipA oligomer formation.

This is further supported by analysis of mutants with Y35, K114, E122, and E150 substitutions, each of which is within a cytoplasmic domain, which showed that these amino acids are also required for intracellular replication in both macrophages and epithelial cells, as well as for suppression of the proinflammatory immune response. Unlike the RipAΔaa105-151 cytoplasmic domain deletion mutant, the single amino acid changes were not sufficient to prevent RipA oligomerization, suggesting that the interactions are mediated by multiple amino acids or that the individual amino acids are involved in some other aspect of RipA function. In terms of the first cytoplasmic domain, the inability to determine the involvement of amino acids 4 to 47 in RipA oligomer formation was due to RipAΔaa4-47 decreased cytoplasmic membrane expression. Nevertheless, there is a possibility that the first cytoplasmic domain is involved in the formation of RipA oligomers and even that the two cytoplasmic domains interact. The intragenic suppressor mutation V39A in the E150A mutant restores the ability of the E150A mutant to replicate intracellularly and suppress the IL-1β response. That V39 and E150 are in the first and second cytoplasmic domains, respectively, suggests that the two cytoplasmic domains interact with each other or, alternatively, with another shared substrate. Overall, our data show that both cytoplasmic domains, and even certain amino acids within each domain, are important for RipA function.

The fact that there are other RipA-like proteins in a wide range of mainly less-studied species, including pathogenic, nonpathogenic, Gram-positive, and Gram-negative mycobacteria; soil-dwelling, marine-dwelling, and freshwater-dwelling bacteria; and even one *Archaea* member is intriguing. Stranger still is the fact that RipA proteins have been identified only in select strains of a given species, with the exception being members of the genus *Francisella*, where RipA is conserved among all sequenced species and strains. This could be due in part to a lack of genome sequences for a given species, or RipA could be a truly rare protein or one for which there are functional homologs that share little protein sequence homology. So far, RipA-like proteins have been identified in only four strains of pathogenic bacterial species: *Mycobacterium avium*, which can cause disease in birds, as well as children, the elderly, and the immunocompromised; *Streptomyces scabiei*, which causes disease in plants; *Aeromonas caviae*, which is a cause of gastrointestinal disease in humans; and *Actinomyces odontolyticus*, which is an opportunistic pathogen causing invasive disease in elderly or immunocompromised patients with advanced dental cavities. Whether or not these RipA-like proteins play a role in pathogenesis is not known. Since we know that RipA is an important *F. tularensis* virulence factor, it is possible that the function of RipA will represent a virulence mechanism that is conserved among pathogenic bacteria. An alternative, and equally exciting, possibility is that RipA functions as a novel virulence mechanism unique to *Francisella*. Since the bacteria in which other RipA-like proteins are found are so varied in classification, it will be interesting to determine if there are differences in the function of RipA among pathogenic and nonpathogenic strains. The fact that a virulence gene homolog is found in environmental bacteria is not unprecedented. A recent *in silico* analysis of marine bacterial genomes for virulence factors revealed an abundance of well-characterized virulence genes, including pathogenicity islands and genes encoding secretion systems and toxins, represented among the strains analyzed (32). Genes encoding virulence factors are also widely distributed among soil bacteria (4). Perhaps

RipA belongs to a novel family of proteins that will be revealed as more strains are sequenced and deposited into NCBI, resulting in the identification of more RipA-like proteins. Overall, determination of the function of RipA is relevant not only for understanding the virulence of *F. tularensis* but also perhaps for understanding the function of a potential class of proteins distributed throughout the bacterial kingdom.

REFERENCES

1. **Birdsell DN, et al.** 2009. Francisella tularensis subsp. novicida isolated from a human in Arizona. BMC Res. Notes **2**:223.
2. **Bosio CM, Dow SW.** 2005. Francisella tularensis induces aberrant activation of pulmonary dendritic cells. J. Immunol. **175**:6792–6801.
3. **Bosio CM, Bielefeldt-Ohmann H, Belisle JT.** 2007. Active suppression of the pulmonary immune response by Francisella tularensis Schu4. J. Immunol. **178**:4538–4547.
4. **Casadevall A.** 2006. Cards of virulence and the global virulome for humans. Microbe **1**:359–364.
5. **Centers for Disease Control and Prevention.** 2009. Tularemia—Missouri, 2000-2007. MMWR Morb. Mortal. Wkly. Rep. **58**:744–748.
6. **Centers for Disease Control and Prevention.** 2005. Tularemia transmitted by insect bites—Wyoming, 2001-2003. MMWR Morb. Mortal. Wkly. Rep. **54**:170–173.
7. **Chamberlain RE.** 1965. Evaluation of live tularemia vaccine prepared in a chemically defined medium. Appl. Microbiol. **13**:232–235.
8. **Chase JC, Celli J, Bosio CM.** 2009. Direct and indirect impairment of human dendritic cell function by virulent Francisella tularensis Schu S4. Infect. Immun. **77**:180–195.
9. **Clarridge JE, III, et al.** 1996. Characterization of two unusual clinically significant *Francisella* strains. J. Clin. Microbiol. **34**:1995–2000.
10. **Clemens DL, Lee BY, Horwitz MA.** 2005. *Francisella tularensis* enters macrophages via a novel process involving pseudopod loops. Infect. Immun. **73**:5892–5902.
11. **Clemens DL, Lee BY, Horwitz MA.** 2004. Virulent and avirulent strains of *Francisella tularensis* prevent acidification and maturation of their phagosomes and escape into the cytoplasm in human macrophages. Infect. Immun. **72**:3204–3217.
12. **Daley DO, et al.** 2005. Global topology analysis of the Escherichia coli inner membrane proteome. Science **308**:1321–1323.
13. **Dennis DT, et al.** 2001. Tularemia as a biological weapon: medical and public health management. JAMA **285**:2763–2773.
14. **Derman AI, Beckwith J.** 1991. *Escherichia coli* alkaline phosphatase fails to acquire disulfide bonds when retained in the cytoplasm. J. Bacteriol. **173**:7719–7722.
15. **Drew D, et al.** 2002. Rapid topology mapping of Escherichia coli inner-membrane proteins by prediction and PhoA/GFP fusion analysis. Proc. Natl. Acad. Sci. U. S. A. **99**:2690–2695.
16. **Fuller JR, Kijek TM, Taft-Benz S, Kawula TH.** 2009. Environmental and intracellular regulation of Francisella tularensis ripA. BMC Microbiol. **9**:216.
17. **Fuller JR, et al.** 2008. RipA, a cytoplasmic membrane protein conserved among *Francisella* species, is required for intracellular survival. Infect. Immun. **76**:4934–4943.
18. **Hall JD, Craven RR, Fuller JR, Pickles RJ, Kawula TH.** 2007. *Francisella tularensis* replicates within alveolar type II epithelial cells in vitro and in vivo following inhalation. Infect. Immun. **75**:1034–1039.
19. **Hall JD, et al.** 2008. Infected-host-cell repertoire and cellular response in the lung following inhalation of *Francisella tularensis* Schu S4, LVS, or U112. Infect. Immun. **76**:5843–5852.
20. **Hollis DG, et al.** 1989. *Francisella philomiragia* comb. nov. (formerly *Yersinia philomiragia*) and *Francisella tularensis* biogroup novicida (formerly *Francisella novicida*) associated with human disease. J. Clin. Microbiol. **27**:1601–1608.
21. **Horton RM, Hunt HD, Ho SN, Pullen JK, Pease LR.** 1989. Engineering hybrid genes without the use of restriction enzymes: gene splicing by overlap extension. Gene **77**:61–68.
22. **Huang MT, et al.** 2010. Deletion of ripA alleviates suppression of the inflammasome and MAPK by Francisella tularensis. J. Immunol. **185**:5476–5485.
23. **Kandemir B, Erayman I, Bitirgen M, Aribas ET, Guler S.** 2007. Tularemia presenting with tonsillopharyngitis and cervical lymphadenitis: report of two cases. Scand. J. Infect. Dis. **39**:620–622.
24. **Keim P, Johansson A, Wagner DM.** 2007. Molecular epidemiology, evolution, and ecology of Francisella. Ann. N. Y. Acad. Sci. **1105**:30–66.
25. **Larssen KW, et al.** 2011. Outbreak of tularaemia in central Norway, January to March 2011. Euro Surveill. **16**:19828.
26. **Leelaporn A, Yongyod S, Limsrivanichakorn S, Yungyuen T, Kiratisin P.** 2008. Francisella novicida bacteremia, Thailand. Emerg. Infect. Dis. **14**:1935–1937.
27. **LoVullo ED, Sherrill LA, Perez LL, Pavelka MS, Jr.** 2006. Genetic tools for highly pathogenic Francisella tularensis subsp. tularensis. Microbiology **152**:3425–3435.
28. **Lundström JO, et al.** 2011. Transstadial transmission of Francisella tularensis holarctica in mosquitoes, Sweden. Emerg. Infect. Dis. **17**:794–799.
29. **Marchette NJ, Nicholes PS.** 1961. Virulence and citrulline ureidase activity of *Pasteurella tularensis*. J. Bacteriol. **82**:26–32.
30. **Münnich D, Lakatos M.** 1979. Clinical, epidemiological and therapeutical experience with human tularaemia: the role of hamster hunters. Infection **7**:61–63.
31. **Padeshki PI, Ivanov IN, Popov B, Kantardjiev TV.** 2010. The role of birds in dissemination of Francisella tularensis: first direct molecular evidence for bird-to-human transmission. Epidemiol. Infect. **138**:376–379.
32. **Persson OP, et al.** 2009. High abundance of virulence gene homologues in marine bacteria. Environ. Microbiol. **11**:1348–1357.
33. **Rapp M, et al.** 2004. Experimentally based topology models for E. coli inner membrane proteins. Protein Sci. **13**:937–945.
34. **Reese SM, et al.** 2010. Transmission dynamics of Francisella tularensis subspecies and clades by nymphal Dermacentor variabilis (Acari: Ixodidae). Am. J. Trop. Med. Hyg. **83**:645–652.
35. **Saslaw S, Eigelsbach HT, Prior JA, Wilson HE, Carhart S.** 1961. Tularemia vaccine study. II. Respiratory challenge. Arch. Intern. Med. **107**:702–714.
36. **Scheftel JM, et al.** 2010. Tularaemia in Minnesota: case report and brief epidemiology. Zoonoses Public Health **57**:e165–e169.
37. **Siret V, et al.** 2006. An outbreak of airborne tularaemia in France, August 2004. Euro Surveill. **11**:58–60.
38. **Sonnhammer EL, von Heijne G, Krogh A.** 1998. A hidden Markov model for predicting transmembrane helices in protein sequences. Proc. Int. Conf. Intell. Syst. Mol. Biol. **6**:175–182.
39. **Spyropoulos IC, Liakopoulos TD, Bagos PG, Hamodrakas SJ.** 2004. TMRPres2D: high quality visual representation of transmembrane protein models. Bioinformatics **20**:3258–3260.
40. **Telepnev M, Golovliov I, Sjostedt A.** 2005. Francisella tularensis LVS initially activates but subsequently down-regulates intracellular signaling and cytokine secretion in mouse monocytic and human peripheral blood mononuclear cells. Microb. Pathog. **38**:239–247.
41. **Telepnev M, Golovliov I, Grundstrom T, Tarnvik A, Sjostedt A.** 2003. Francisella tularensis inhibits Toll-like receptor-mediated activation of intracellular signalling and secretion of TNF-alpha and IL-1 from murine macrophages. Cell. Microbiol. **5**:41–51.
42. **Teutsch SM, et al.** 1979. Pneumonic tularemia on Martha's Vineyard. N. Engl. J. Med. **301**:826–828.
43. **Triebenbach AN, et al.** 2010. Detection of Francisella tularensis in Alaskan mosquitoes (Diptera: Culicidae) and assessment of a laboratory model for transmission. J. Med. Entomol. **47**:639–648.